Conformability of a Thin Elastic Membrane Laminated on a Rigid Substrate With Corrugated Surface

Shutao Qiao, Jean-Baptiste Gratadour, Liu Wang, and Nanshu Lu

***Abstract*— When laminating a thin elastic membrane on a substrate with surface roughness, three scenarios can happen: 1) fully conformed, i.e., the membrane completely follows the surface morphology of the substrate without any interfacial gap; 2) partially conformed; and 3) nonconformed, i.e., the membrane remains flat if gravity is not concerned. Good conformability can enhance effective membrane-to-substrate adhesion and can facilitate heat/signal transfer across the interface, which are of great importance for micromembranes or nanomembranes transferred on target substrates and for flexible electronics laminated on rough biotissues. To reveal the governing parameters in this problem and to predict the conformability, energy minimization method is implemented with two different interfacial models, adhesion energy versus traction-separation relation. Depending on the complexity of the models, one to four dimensionless governing parameters have been identified to analytically predict the conformability status and the point of delamination if partial conformability is expected. In any case, partial conformability is achieved only when membrane energy is considered.**

***Index Terms*— Adhesion, conformability, rough surfaces.**

I. Introduction

ALL surfaces have roughness. For example, the root-mean-squared (rms) roughness of high-end polished silicon wafers can be as small as 0.3 nm [1] and the rms surface roughness of human skin ranges from 0.03 to 45 μm [2]. When laminating a thin membrane on a substrate with surface roughness, three scenarios can happen: 1) fully conformed (FC) [Fig. 1(a)], i.e., the membrane completely follows the surface morphology of the substrate without any interfacial gap; 2) partially conformed (PC) [Fig. 1(b)], i.e., a part of the membrane forms intimate contact with the substrate surface while other part is suspended; and 3) nonconformed (NC) [Fig. 1(c)], i.e., the membrane remains flat if gravity is not concerned.

Conformability is important for the adhesion between micromembranes or nanomembranes and their supporting substrates. Many crystalline inorganic semiconductor thin films have to be grown on certain crystalline substrates and then transferred from the growth substrate to the target substrate for device fabrication. For example, large-area monolayer graphene has to be epitaxially grown on a catalyst copper substrate through chemical vapor deposition [3]. To build a device, graphene has to be transferred from the conductive copper to an insulating substrate, which can be rigid substrates like SiO_2 on silicon wafers or flexible substrates like Kapton or polyethylene terephthalate (PET) sheets. Depending on the surface morphology of the substrate, adhesion of monolayer graphene transferred to foreign substrates can significantly vary: from 0.357 J/m^2 on silicon wafer with an rms roughness of 0.3 nm [1] to 0.51 J/m^2 on copper film (a foreign copper, not the growth copper) with an rms roughness of 0.15 mm [4], both of which are measured by the same research group. Since atomically thick graphene can conform to almost all surfaces but copper surface rms is much larger than silicon surface, the higher effective adhesion energy between graphene and copper may come from larger effective interface contact area due to conformability if van der Waals interaction is assumed for both interfaces. Membrane thickness also affects adhesion. For example, while monolayer graphene to SiO_2 adhesion is measured to be 0.45 J/m^2, two to five layer graphene is only 0.31 J/m^2 [5]. An analytical model has been developed to reveal how substrate surface roughness and membrane thickness may affect the conformability and hence adhesion between graphene and their substrates [6]. The interface is modeled by van der Waals interaction that is

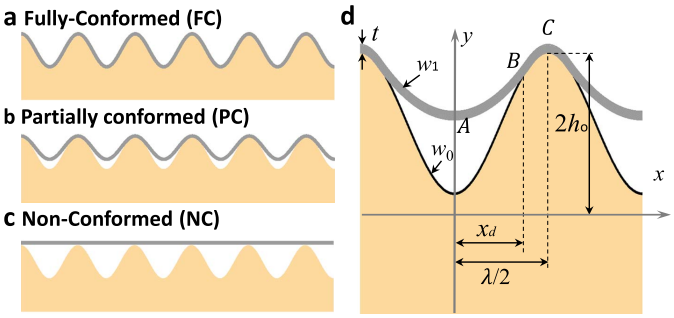

Fig. 1. (a)–(c) Three possible conformability statuses when a thin membrane is laminated on a sinusoidally rough rigid substrate. (d) Magnified view of (b) with geometric parameters labeled. x_d is the horizontal projection of the delaminated part.

Manuscript received March 1, 2015; accepted June 10, 2015. This work was supported by the National Science Foundation under Award 1301335. Recommended for publication by Associate Editor H. Jiang upon evaluation of reviewers' comments. *(Corresponding author: Nanshu Lu.)*

S. Qiao, L. Wang, and N. Lu are with the Center for Mechanics of Solids, Structures and Materials, Department of Aerospace Engineering and Engineering Mechanics, Texas Materials Institute, The University of Texas at Austin, Austin, TX 78712 USA (e-mail: shutaoqiao@utexas.edu; leo1993@utexas.edu; nanshulu@utexas.edu).

J.-B. Gratadour is with the Graduate School of Engineering, Arts et Métiers ParisTech, Paris 75013, France (e-mail: jean-baptiste.gratadour@gadz.org).

Color versions of one or more of the figures in this paper are available online at http://ieeexplore.ieee.org.

Digital Object Identifier 10.1109/TCPMT.2015.2453319

appropriate for graphene–substrate interaction but other traction-separation relations (TSR) are not explored. The reduced adhesion of thicker graphene is attributed to less conformability but the area of contact is not predicted in this model. Because of the interplay between conformability and adhesion, conformability-based metrology has been applied to estimate the interface adhesion between graphene and precorrugated polydimethylsiloxane substrate [7].

Conformability of thin membranes on rough substrate is also critical for biointegrated electronics [8], where flexible and stretchable electronic sensing and therapeutic devices are in intimate contact with biotissues for disease monitoring, diagnosis, and even treatment. Examples of biointegrated electronic sheets or webs include soft electrodes on the cortex [9], epicardial sensing and actuation web [10], as well as epidermal electronic systems [11]. High conformability between device sheets and biotissues not only affords large-area mapping capability [9] and superior signal-to-noise ratio [12], but also promotes efficient heat transfer for temperature sensing or ablation treatment [10]. Mechanistic understanding of how electronic sheets conform to biosurfaces can provide rational guidance for the design of future biointegrated electronics. Analytical models for the conformability of epidermal electronics on human skin have been developed and the divide between fully conformal and nonconformal has been established and found consistecy with the experimental observations [13], [14]. However, partially conformed situations [Fig. 1(b)] have never been discussed whereas they can be clearly seen in experiments [12]. More models are needed to predict this scenario and the actual contact area.

In this paper, energy method will be used to develop four analytical models of an elastic membrane conforming to a sinusoidally rough substrate and the dimensionless governing parameters will be revealed for each model. We limit ourselves to rigid substrates in this paper with the intension of extending these models to soft, corrugated substrates in the future. Two different ways of defining conformability will be discussed when modeling the interface with adhesion energy versus TSR, as will be discussed in Sections II and III, respectively. When adhesion energy is used, three models with different assumptions on the substrate roughness and the membrane energy will be developed and compared. Conclusions are presented in Section IV.

II. Model 1—Interface Modeled by Work of Adhesion

When an elastic membrane is laminated on a sinusoidally corrugated rigid substrate, a magnified partially conformed configuration is shown in Fig. 1(d). The membrane is modeled as a uniform linear elastic sheet with plane strain modulus $\bar{E}$ and thickness t. The substrate is assumed to be rigid, so that it does not deform or store any elastic energy. When an xy coordinate is established as shown, the surface morphology of the substrate can be simply characterized by a sinusoidal equation

$$w_0(x) = h_0\left(1-\cos\frac{2\pi x}{\lambda}\right) \tag{1}$$

where h_0 and λ denote the amplitude and wavelength of the substrate surface, respectively. If we use x_d to denote the horizontal projection of the delaminated region in Fig. 1(d), then $x_d = 0$ means fully conformed [Fig. 1(a)], $0 < x_d < \lambda/2$ means partially conformed [Fig. 1(b)], and $x_d = \lambda/2$ means nonconformed [Fig. 1(c)].

The profile of a partially conformed membrane, $w_1(x)$ as shown in Fig. 1(d), is going to be sectional: from A to B, i.e., when $0 \le x \le x_d$, the membrane is suspended and $w_1(x)$ should take a parabolic shape if pure bending is assumed, i.e., normal strain in the membrane is neglected; from B to C, i.e., when $x_d \le x \le \lambda/2$, the membrane fully conforms to the substrate and $w_1(x)$ should be the same as $w_0(x)$. Therefore, $w_1(x)$ can be expressed as

$$w_1(x) = \begin{cases} ax^2+b, & 0 \le x \le x_d \\ h_0\left(1-\cos\frac{2\pi x}{\lambda}\right), & x_d \le x \le \lambda/2. \end{cases} \tag{2}$$

Applying the continuity condition at point B where both the profile and slope of the membrane should be continuous, i.e., $w_1(x_d) = w_0(x_d)$ and $w_1'(x_d) = w_0'(x_d)$, we can solve the coefficients a and b in (2) and obtain the profile of the thin film from A to B as

$$w_1(x) = h_0\left[\frac{\pi}{\lambda x_d}\sin\left(\frac{2\pi x_d}{\lambda}\right)\left(x^2-x_d^2\right)+1-\cos\left(\frac{2\pi x_d}{\lambda}\right)\right] \quad 0 \le x \le x_d. \tag{3}$$

The only unknown in (3) is x_d, which means solving x_d can fully determine the membrane profile. To solve x_d, we use energy minimization method.

Since the rigid substrate does not store any elastic energy, the total energy U_{total} of this system can be written as

$$U_{\text{total}} = U_{\text{bending}} + U_{\text{membrane}} + U_{\text{adhesion}} \tag{4}$$

where U_{bending} is the bending energy of the membrane, U_{membrane} is the membrane energy associated with normal strain in the membrane, and U_{adhesion} is the adhesion energy between the membrane and the substrate. Each individual energy can be analytically expressed as follows.

The bending energy of the membrane (per unit length along the wavelength direction) is given by

$$U_{\text{bending}} = \frac{2}{\lambda}\left[\frac{1}{2}\int_A^B \bar{E}I\kappa_1^2 ds + \frac{1}{2}\int_B^C \bar{E}I\kappa_0^2 ds\right] \tag{5}$$

where, $\bar{E}I = \bar{E}t^3/12$ is the bending stiffness of the membrane and κ is its curvature. We use subscript 1 to represent the detached part of the membrane and subscript 0 to represent the adhered part of the membrane.

The membrane energy can be written as

$$U_{\text{membrane}} = \frac{2}{\lambda}\left[\frac{1}{2}\int_A^B \bar{E}t\epsilon_1^2 ds + \frac{1}{2}\int_B^C \bar{E}t\epsilon_0^2 ds\right] \tag{6}$$

where $\epsilon_1(x) = (1+w_1'^2)^{1/2}-1$ and $\epsilon_0(x) = (1+w_0'^2)^{1/2}-1$ are the normal strains in the detached and adhered sections of the membrane, respectively.

Adhesion between the membrane and the substrate actually reduces the system energy so it should be negative. Given the

membrane–substrate interface work of adhesion γ, adhesion energy becomes

$$U_{\text{adhesion}} = -\frac{2}{\lambda}\int_B^C \gamma\, ds. \tag{7}$$

Minimization of the total energy as given in (4) can then yields equilibrium contact point x_d as a function of the substrate wavelength and amplitude, membrane thickness and modulus, as well as membrane–substrate interface work of adhesion. When making different assumptions about κ and U_{membrane}, three different models are developed and compared.

A. Model 1.1—Small Roughness With Membrane Energy Neglected

Starting from the simplest scenario, we consider the substrate to have a small roughness, i.e., $h_0/\lambda \ll 1$. In this case, the membrane is going to experience small deflection even when it fully conforms to the substrate, hence $\kappa_i \approx w_i''$ $(i = 0, 1)$, $ds \approx dx$, and $w_i' \approx 0$ are adopted. As a result, $\epsilon_i(x) \approx 0$ in the membrane and $U_{\text{membrane}} = 0$. The three energy components hence can be written as

$$\begin{aligned} U_{\text{bending}} &\approx \frac{\bar{E}I}{\lambda}\left[\int_0^{x_d}\left(w_1''\right)^2 dx + \int_{x_d}^{\lambda/2}\left(w_0''\right)^2 dx\right] \\ U_{\text{membrane}} &= 0 \\ U_{\text{adhesion}} &\approx -\gamma\left(1 - \frac{2x_d}{\lambda}\right). \end{aligned} \tag{8}$$

The total energy then becomes

$$\begin{aligned} U_{\text{total}} = \frac{\bar{E}I}{\lambda}\Bigg[&4h_0^2\frac{\pi^2}{\lambda^2 x_d}\sin^2\left(\frac{2\pi x_d}{\lambda}\right) \\ &+ h_0^2\frac{16\pi^4}{\lambda^4}\left(\frac{\lambda - 2x_d}{4} - \frac{\lambda}{8\pi}\sin\left(\frac{4\pi x_d}{\lambda}\right)\right)\Bigg] \\ &- \gamma\left(1 - 2\frac{x_d}{\lambda}\right). \end{aligned} \tag{9}$$

Through dimensional analysis, the normalized total energy can be written as

$$\begin{aligned} \hat{U} &= \frac{U_{\text{total}}\lambda^4}{4\pi^2 h_0^2 \bar{E}I} \\ &= \frac{2}{\hat{x}_d}\sin^2(\pi\hat{x}_d) + \left(\pi^2 - \frac{\alpha}{\beta^2}\right)(1 - \hat{x}_d) - \frac{\pi}{2}\sin(2\pi\hat{x}_d) \end{aligned} \tag{10}$$

where $\alpha = \gamma\lambda^2/(\bar{E}I)$, $\beta = 2\pi h_0/\lambda$, and $\hat{x}_d = 2x_d/\lambda$ are the dimensionless variables and $\alpha/\beta^2 = \gamma\lambda^4/(4\pi^2 h_0^2 \bar{E}I)$.

It is evident from (10) that the normalized total energy is only determined by α/β^2 and $\hat{x}_d$. Fig. 2(a) plots $\hat{U}$ as a function of $\hat{x}_d$ with different α/β^2 values. For all possible $\hat{U}(\hat{x}_d)$, minimal energy falls at either $\hat{x}_d = 0$ or $\hat{x}_d = 1$, which means that depending on α/β^2, the conformability can be tuned between full or none, but not partial. The critical condition can be determined by $\hat{U}(\hat{x}_d = 0) = \hat{U}(\hat{x}_d = 1)$, which yields

$$\alpha/\beta^2 = \pi^2. \tag{11}$$

When $\alpha/\beta^2 > \pi^2$, as shown in Fig. 2(a), the total energy would minimize at $\hat{x}_d = 0$ and full conformability can be achieved, sometimes with a little external help to overcome the energy hump from $\hat{x}_d = 1$ to $\hat{x}_d = 0$. When $\alpha/\beta^2 < \pi^2$, as shown in Fig. 2(a), the total energy would minimize at $\hat{x}_d = 1$ and the membrane is predicted to stay nonconformed at all. The fact that larger α/β^2 yields better conformability indicates that a soft and thin film ($\bar{E}I$ is small) is more likely to conform to sticky substrates (large γ) with long wavelength (large λ) and small amplitude (small h_0), which fully agrees with our intuition. The importance of λ is manifested by the power of 4 in the governing parameter α/β^2.

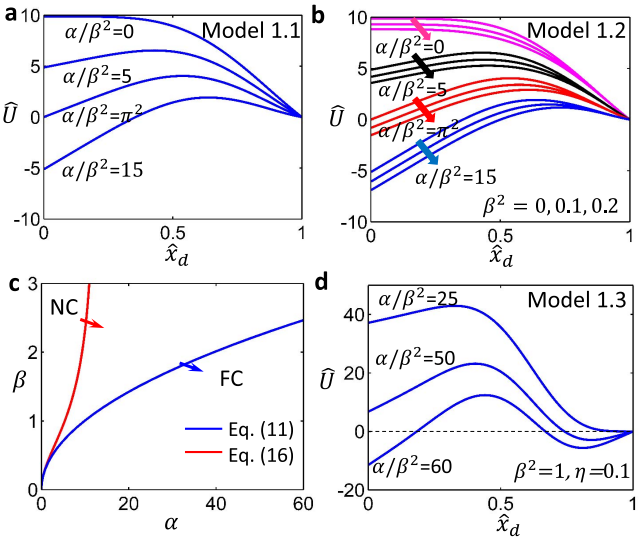

Fig. 2. Normalized total energy as a function of x_d for Models (a) 1.1 (10), (b) 1.2 (15), and (d) 1.3 (19). (c) Blue and red curves, plotted from (11) and (17), represent the boundary between FC and NC in Models 1.1 and 1.2, respectively.

B. Model 1.2—Large Roughness With Membrane Energy Neglected

In Model 1.1, small roughness ($h_0/\lambda \ll 1$) is assumed. In this model, we relax this assumption and therefore have to adopt the full expressions of the curvature κ

$$\kappa_i = \frac{w_i''}{\left[1 + \left(w_i'\right)^2\right]^{3/2}} \tag{12}$$

and the curve length ds

$$ds = \sqrt{1 + \left(w_i'\right)^2}\,dx. \tag{13}$$

Still pretending membrane energy is negligible, the three different energies become

$$\begin{aligned} U_{\text{bending}} &= \frac{\bar{E}I}{\lambda}\left[\int_0^{x_d}\frac{\left(w_1''\right)^2}{\left[1 + \left(w_1'\right)^2\right]^3}dx \right. \\ &\qquad \left. + \int_{x_d}^{\lambda/2}\frac{\left(w_0''\right)^2}{\left[1 + \left(w_0'\right)^2\right]^3}dx\right] \\ U_{\text{membrane}} &= 0 \\ U_{\text{adhesion}} &= -\frac{2\gamma}{\lambda}\int_{x_d}^{\lambda/2}\sqrt{1 + \left(w_0'\right)^2}\,dx. \end{aligned} \tag{14}$$

After integration and nondimensionalization, the total energy becomes

$$\begin{aligned}\hat{U} &= \frac{U_{\text{total}}\lambda^4}{4\pi^2 h_0^2 \bar{E} I} \\ &= \frac{2(3+2\beta^2\sin^2(\pi\hat{x}_d))\sin^2(\pi\hat{x}_d) - \pi\hat{x}_d\sin(2\pi\hat{x}_d)}{3\hat{x}_d(1+\beta^2\sin^2(\pi\hat{x}_d))^{\frac{3}{2}}} \\ &\quad - \frac{\pi}{3}\frac{1+2\beta^2}{1+\beta^2}\frac{\sin(2\pi\hat{x}_d)}{(1+\beta^2\sin^2(\pi\hat{x}_d))^{\frac{1}{2}}} \\ &\quad + \frac{2\pi}{3}\frac{F(\pi\hat{x}_d,-\beta^2)-2K(-\beta^2)}{\beta^2} \\ &\quad + \frac{2E(-\beta^2)-E(\pi\hat{x}_d,-\beta^2)}{\beta^2}\left(\frac{2\pi}{3}\frac{1+2\beta^2}{1+\beta^2}-\frac{\alpha}{\pi}\right) \end{aligned} \tag{15}$$

where $F(\phi,k)$ and $E(\phi,k)$ are the incomplete elliptic integral of the first and second kinds, respectively. $K(k)=F(\pi/2,k)$ and $E(k)=E(\pi/2,k)$ are the complete elliptic integral of the first and second kinds, respectively.

There are only three independent dimensionless variables appear in the nondimensionalized total energy given in (15): $\alpha = \gamma\lambda^2/(\bar{E}I)$, $\beta = 2\pi h_0/\lambda$, and $\hat{x}_d = 2x_d/\lambda$. At given α and β, $\hat{U}$ can be plotted as a function of $\hat{x}_d$, as shown in Fig. 2(b). Curves with the same color share the same α/β^2 values, whereas the three different curves within one bunch have different values of β, with an arrow indicating increasing β. The curves with $\beta > 0$ in Fig. 2(b) can fully overlap with the curves in Fig. 2(a), indicating that when the roughness is small, Model 1.1 can be recovered from Model 1.2. Similar to Fig. 2(a), the minimal energy points fall either at $\hat{x}_d = 0$ or $\hat{x}_d = 1$ in Fig. 2(b), which suggests that no partial conformability can be predicted by Model 1.2 either. The critical condition separating full conformability and nonconformability is

$$\alpha = \frac{2\pi^2}{3}\left[\frac{1+2\beta^2}{1+\beta^2} - \frac{K(-\beta^2)}{E(-\beta^2)}\right]. \tag{16}$$

Again, the conformability can be fully captured by an equation of α and β similar to (11). When $\beta \to 0$, (16) recovers (11). When plotting (11) and (16) in the same α–β graph as shown in Fig. 2(c), both curves suggest that smaller β and larger α can afford better conformability. Also note that when β is small, the two curves fully overlap but when β is large, (11) (Model 1.1) defines a smaller zone of full conformability than (16) (Model 1.2). The reason is that in Model 1.1, the curvature κ and contact area ds are highly simplified because of small roughness assumption, resulting in a larger curvature and smaller contact area than those used in Model 1.2, which means that larger bending energy while smaller adhesion energy are used in Model 1.1. Since bending energy penalizes conformability whereas adhesion promotes it, it is more difficult to reach full conformability in Model 1.1 than in Model 1.2.

C. Model 1.3—Large Deflection With Membrane Energy Considered

While Model 1.2 intentionally neglects the membrane energy, in this model, the membrane energy will be added by substituting (13) into (6):

$$\begin{aligned} U_{\text{membrane}} &= \frac{2}{\lambda}\left[\frac{1}{2}\int_0^{x_d}\bar{E}t\left(\sqrt{1+{w_1'}^2}-1\right)^2\left[1+\left(w_1'\right)^2\right]^{1/2}dx \right. \\ &\quad \left. + \frac{1}{2}\int_{x_d}^{\lambda/2}\bar{E}t\left(\sqrt{1+{w_0'}^2}-1\right)^2\left[1+\left(w_0'\right)^2\right]^{1/2}dx\right]. \end{aligned} \tag{17}$$

The nondimensionalized membrane energy can be analytically expressed as

$$\begin{aligned}\hat{U}_{\text{membrane}} &= \frac{U_{\text{membrane}}\lambda^4}{4\pi^2 h_0^2\bar{E}I} = \frac{12}{\eta^2}\left\{\frac{7\hat{x}_d}{16\beta^2}\frac{\sinh^{-1}(\beta\sin(\pi\hat{x}_d))}{\beta\sin(\pi\hat{x}_d)}\right. \\ &\quad - \frac{\hat{x}_d}{3}\sin^2(\pi\hat{x}_d) + \frac{\hat{x}_d}{8\beta^2}(1+\beta^2\sin^2(\pi\hat{x}_d))^{3/2} - \frac{1}{\beta^2} \\ &\quad - \frac{1-\hat{x}_d}{2} + \frac{7+2\beta^2}{6\pi\beta^2}[2E(-\beta^2)-E(\pi\hat{x}_d,-\beta^2)] \\ &\quad - \frac{1+\beta^2}{6\pi\beta^2}[2K(-\beta^2)-F(\pi\hat{x}_d,-\beta^2)] - \frac{\sin(2\pi\hat{x}_d)}{4\pi} \\ &\quad \left. + \left(\frac{7\hat{x}_d}{16\beta^2}+\frac{\sin(2\pi\hat{x}_d)}{12\pi}\right)\sqrt{1+\beta^2\sin^2(\pi\hat{x}_d)}\right\} \end{aligned} \tag{18}$$

where $\eta = t/\lambda$, which is a new dimensionless variable that appears due to the consideration of membrane energy. Adopting the same bending and adhesion energies as Mode 1.2, the normalized total energy of Model 1.3 is given by the summation of (15) and (18). The total energy now is a function of four dimensionless variables, α, β, η, and $\hat{x}_d$. To plot a $\hat{U} \sim \hat{x}_d$ curve, we need to fix the other three variables, like what Fig. 2(d) does. It is evident that unlike Fig. 2(a) and (b), in Fig. 2(d), some $\hat{U} \sim \hat{x}_d$ curves show local minimum valleys at $0 < \hat{x}_d < 1$, which indicates the possibility of partial conformability. It is important to point out that in Model 1.3, full conformability can only be achieved when α/β^2 is much larger than those required for Models 1.1 and 1.2, as the strain energy can well exceed the bending energy, which requires significant adhesion energy to overcome.

Since

$$\alpha = \frac{\gamma\lambda^2}{\bar{E}I} = \frac{\gamma}{\bar{E}\lambda}\frac{12}{\eta^3} \tag{19}$$

for the sake of physical interpretation, we replace α with $\gamma/\bar{E}\lambda$ and use $\{\gamma/\bar{E}\lambda, h_0/\lambda, t/\lambda\}$ instead of $\{\alpha,\beta,\eta\}$ to describe the normalized total energy. For any possible combination of $\{\gamma/\bar{E}\lambda, h_0/\lambda, t/\lambda\}$, the minimum $\hat{U}$ can be obtained as well as the corresponding $\hat{x}_d$, which not only predicts the conformability outcome, but also the conformed area, as shown in both Figs. 3 and 4. $\gamma/\bar{E}\lambda$ is set to be 0.01 in Fig. 3(a) and 0.2 in Fig. 3(b) and the $\hat{x}_d$ corresponding to the minimum $\hat{U}$ is plotted for various substrate roughnesses (h_0/λ) and film thickness ratios (t/λ). By increasing $\gamma/\bar{E}\lambda$, i.e., enhancing the interface work of adhesion or decreasing the film stiffness, nonconformed configuration could be avoided. Fig. 4 predicts the conformability outcome as a function of three

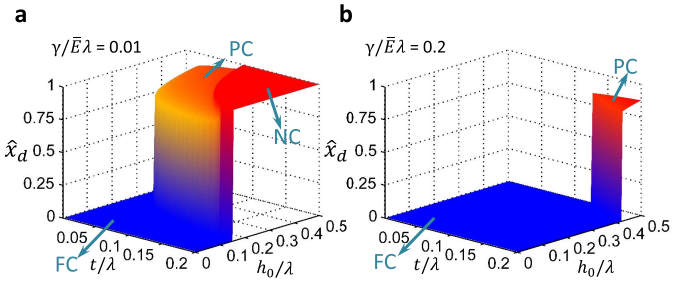

Fig. 3. $\hat{x}_d$ that corresponds to the minimum $\hat{U}$ is plotted for various substrate roughnesses (h_0/λ) and film thickness ratios (t/λ) with (a) $\gamma/\bar{E}\lambda = 0.01$ and (b) $\gamma/\bar{E}\lambda = 0.2$.

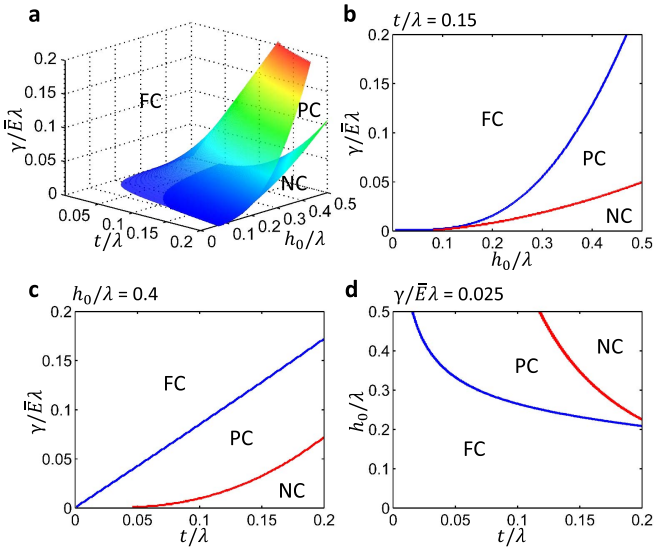

Fig. 4. (a) 3-D critical surfaces dividing FC/PC and PC/NC given by Model 1.3. (b)–(d) Cross-sectional views of (a) by making planer cuts at (b) $t/\lambda = 0.15$, (c) $h_0/\lambda = 0.4$, and (d) $\gamma/\bar{E}\lambda = 0.025$. The boundaries in (b)–(d) between FC and PC and between PC and NC are plotted in blue and red curves, respectively.

variables $\gamma/\bar{E}\lambda$, h_0/λ, and t/λ. By numerically solving the minimization problem of Model 1.3, the 3-D plot in Fig. 4(a) shows the critical surfaces dividing FC/PC and PC/NC. Cross-sectional views of the 3-D critical surfaces can be achieved by making planar cuts at $t/\lambda = 0.15$, $h_0/\lambda = 0.4$, and $\gamma/\bar{E}\lambda = 0.025$, respectively, and are shown in Figs. 4(b)–(d). Again, conformability can be enhanced using thinner and softer membranes, reducing the substrate amplitude, and enlarging the substrate wavelength and interface work of adhesion.

III. Model 2—Interface Modeled by TSR

In Section II (Model 1), membrane-substrate adhesion is only characterized by the interface work of adhesion γ. A more sophisticated way of looking at interface interaction is the TSR. When a continuous TSR is adopted, and if the membrane profile is also assumed to be sinusoidal, of the same wavelength but a different amplitude from the substrate surface profile [Fig. 5(a)], we can avoid working with sectional functions as what was done in Model 1. Indeed, van der Waals type of continuous TSR

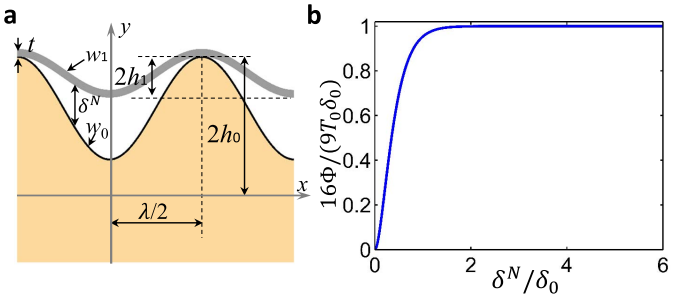

Fig. 5. (a) Schematic for Model 2 where the membrane is assumed to be in sinusoidal shape that has the same wavelength but different amplitudes compared with the substrate. The membrane-substrate separation is denoted by δ^N. The normalized interface potential is plotted as a function of normalized δ^N in (b).

has been used to model the interaction between graphene and rough substrate, so that the conformability can be predicted [15]. Therefore, in Model 2, we adopt a similar approach by employing popular continuous exponential interface potential [16]

$$\Phi(\delta^N) = \frac{9}{16}T_0\delta_0\left[1-\left(1+\frac{16e}{9}\frac{\delta^N}{\delta_0}\right)\exp\left(-\frac{16e}{9}\frac{\delta^N}{\delta_0}\right)\right] \quad (20)$$

where δ^N denotes the separation between the two surfaces in contact, δ_0 is the characteristic separation, T_0 is the maximum interface traction, and e is the base of the natural logarithm. The normalized interface potential is plotted as a function of δ^N/δ_0 in Fig. 5(b). The relation between work of adhesion γ and Φ is given by

$$\gamma = \Phi(\infty) = \frac{9}{16}T_0\delta_0. \quad (21)$$

The membrane profile is assumed to be sinusoidal with the same wavelength as the substrate but amplitude $h_1 = \xi h_0$, where ξ is a dimensionless coefficient and $0 \le \xi \le 1$. In this model, ξ is also an indicator of different status of conformability: $\xi = 1$ corresponds to full conformability and $\xi = 0$ means nonconformed, so $0 < \xi < 1$ represents partial conformability. Since (20) is an asymptotic equation, we actually need to set two arbitrary thresholds of ξ as the criteria to differentiate full conformability and nonconformability from partial conformability: we take $\xi \ge 0.99$ as fully conformed and $\xi \le 0.01$ as nonconformed.

Compared with the three energies in Model 1.3, the only difference in Model 2 is the expression of adhesion energy. Under Model 2 assumption, the profile of the membrane is given by

$$w_1(x) = h_0\left(2-\xi\left(1+\cos\frac{2\pi x}{\lambda}\right)\right). \quad (22)$$

The vertical separation between the surface of the substrate and the membrane is therefore

$$\delta^N(x) = w_1(x) - w_0(x). \quad (23)$$

Therefore, the total adhesion energy (per unit length) in Model 2 now is

$$U_{\text{adhesion}} = \frac{2}{\lambda}\int \Phi(\delta^N(x))dx. \quad (24)$$

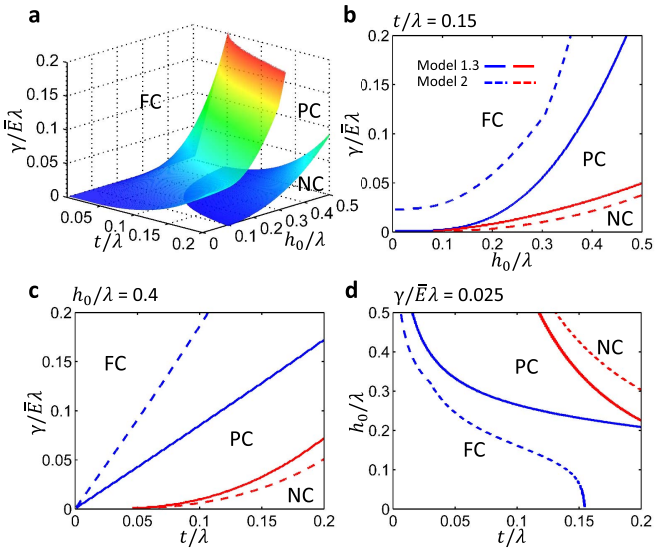

Fig. 6. (a) 3-D critical surfaces dividing FC/PC and PC/NC given by Model 2 when $\delta_0/\lambda = 0.1$ is fixed. (b)–(d) Cross-sectional views of (a) by making planer cuts at (b) $t/\lambda = 0.15$, (c) $h_0/\lambda = 0.4$, and (d) $\gamma/\bar{E}\lambda = 0.025$. The results of Model 1.3 are plotted in solid curves as a comparison.

Applying the same bending energy as given in (14) and the same membrane energy as given in (18), the dimensionless total energy of Model 2 can be expressed in a continuous form:

$$\begin{aligned}\hat{U} &= \frac{U_{\text{total}}\lambda^4}{4\pi^2 h_0^2 \bar{E} I} \\ &= \frac{16}{3\beta^2}\pi\left[\frac{1+2\beta^2\xi^2}{1+\beta^2\xi^2}E(-\beta^2\xi^2) - K(-\beta^2\xi^2)\right] + \frac{12}{\eta^2\beta^2} \\ &\quad \left[-\left(1+\frac{\beta^2\xi^2}{2}\right) + \frac{E(-\beta^2\xi^2)}{\pi} - \frac{1}{3\pi}\sqrt{1+\beta^2\xi^2}\right. \\ &\quad \left.\times\left(-2(2+\beta^2\xi^2)E\left(\frac{\beta^2\xi^2}{1+\beta^2\xi^2}\right) + K\left(\frac{\beta^2\xi^2}{1+\beta^2\xi^2}\right)\right)\right] \\ &\quad + \frac{\alpha}{\beta^2}[1+e^{-k}(-(1+k)I_0(k)+kI_1(k))] \qquad (25)\end{aligned}$$

where $\alpha = \gamma\lambda^2/(\bar{E}I)$, $\beta = 2\pi h_0/\lambda$, $\eta = t/\lambda$, $\xi = h_1/h_0$, and

$$k = \frac{8e}{9\pi}\frac{\lambda}{\delta_0}\beta(1-\xi) \qquad (26)$$

$K(k)$ is the complete elliptic integral of the first kind, $E(k)$ is the complete elliptic integral of the second kind, and $I(k)$ is the Bessel function of the first kind.

In (25), there are five independent dimensionless variables that determine the total energy: α or $\gamma/\bar{E}\lambda$ [see (12)], β or h_0/λ, η or t/λ, k or δ_0/λ [see (26)], and ξ or h_1/h_0. Therefore, with the four dimensionless variables $\{\gamma/\bar{E}\lambda, h_0/\lambda, t/\lambda, \delta_0/\lambda\}$ given, minimization of (25) would yield a solution of ξ.

Similar to Fig. 4(a), the 3-D critical surfaces dividing FC/PC and PC/NC can be numerically obtained by varying $\gamma/\bar{E}\lambda, h_0/\lambda$, and t/λ while fixing $\delta_0/\lambda = 0.1$, as shown in Fig. 6(a). Cross-sectional views of the 3-D critical surfaces are made by taking $t/\lambda = 0.15$, $h_0/\lambda = 0.4$, and $\gamma/\bar{E}\lambda = 0.025$ in Fig. 6(b)–(d). Comparison is made by plotting the same cross-sectional views from Model 1.3 (solid curves) and Model 2 (dashed curves) together in Fig. 6(b)–(d). As we can observe from Fig. 6(b)–(d), for the given δ_0/λ, the conformability obtained from Model 2 behaves similar to that from Model 1.3 but Model 2 generates smaller NC and FC zone while larger PC zone.

IV. Conclusion

Using the method of energy minimization, this paper develops and compares four analytical models with increasing complexity to determine the conformability of thin elastic membranes on rigid substrates with sinusoidal surface morphology. Dimensionless governing parameters have been identified in all models. It has been found that no matter small or large substrate roughness, partial conformability only shows up when the membrane energy is included. All four models point to the same suggestions for enhancing the conformability: 1) thin and soft membrane; 2) substrate surface with long wavelength and small amplitude; and 3) large membrane–substrate interface adhesion. These models are generically applicable to macroscopic as well as microscopic systems as long as continuum mechanics remains valid.

Acknowledgment

The authors would like to thank Prof. K. Liechti for his inspiring discussions.

References

[1] S. R. Na, J. W. Suk, R. S. Ruoff, R. Huang, and K. M. Liechti, "Ultra long-range interactions between large area graphene and silicon," *ACS Nano*, vol. 8, no. 11, pp. 11234–11242, Nov. 2014.

[2] C. P. Hendriks and S. E. Franklin, "Influence of surface roughness, material and climate conditions on the friction of human skin," *Tribol. Lett.*, vol. 37, no. 2, pp. 361–373, Feb. 2010.

[3] X. Li *et al.*, "Large-area synthesis of high-quality and uniform graphene films on copper foils," *Science*, vol. 324, no. 5932, pp. 1312–1314, Jun. 2009.

[4] Z. Cao *et al.*, "A blister test for interfacial adhesion of large-scale transferred graphene," *Carbon*, vol. 69, pp. 390–400, Apr. 2014.

[5] S. P. Koenig, N. G. Boddeti, M. L. Dunn, and J. S. Bunch, "Ultrastrong adhesion of graphene membranes," *Nature Nanotechnol.*, vol. 6, pp. 543–546, Sep. 2011.

[6] W. Gao and R. Huang, "Effect of surface roughness on adhesion of graphene membranes," *J. Phys. D, Appl. Phys.*, vol. 44, no. 45, p. 452001, Nov. 2011.

[7] S. Scharfenberg, D. Z. Rocklin, C. Chialvo, R. L. Weaver, P. M. Goldbart, and N. Mason, "Probing the mechanical properties of graphene using a corrugated elastic substrate," *Appl. Phys. Lett.*, vol. 98, no. 9, p. 091908, Feb. 2011.

[8] D.-H. Kim, R. Ghaffari, N. Lu, and J. A. Rogers, "Flexible and stretchable electronics for biointegrated devices," *Annu. Rev. Biomed. Eng.*, vol. 14, pp. 113–128, Aug. 2012.

[9] D.-H. Kim *et al.*, "Dissolvable films of silk fibroin for ultrathin conformal bio-integrated electronics," *Nature Mater.*, vol. 9, no. 6, pp. 511–517, Jun. 2010.

[10] D.-H. Kim *et al.*, "Electronic sensor and actuator webs for large-area complex geometry cardiac mapping and therapy," *Proc. Nat. Acad. Sci. USA*, vol. 109, no. 49, pp. 19910–19915, Dec. 2012.

[11] D.-H. Kim *et al.*, "Epidermal electronics," *Science*, vol. 333, no. 6044, pp. 838–843, Aug. 2011.

[12] J.-W. Jeong *et al.*, "Materials and optimized designs for human-machine interfaces via epidermal electronics," *Adv. Mater.*, vol. 25, no. 47, pp. 6839–6846, Dec. 2013.

[13] S. Wang *et al.*, "Mechanics of epidermal electronics," *J. Appl. Mech.*, vol. 79, no. 3, pp. 031022-1–031022-6, May 2012.

[14] H. Cheng and S. Wang, "Mechanics of interfacial delamination in epidermal electronics systems," *J. Appl. Mech.*, vol. 81, no. 4, pp. 44501-1–44501-3, Apr. 2014.
[15] Z. H. Aitken and R. Huang, "Effects of mismatch strain and substrate surface corrugation on morphology of supported monolayer graphene," *J. Appl. Phys.*, vol. 107, no. 12, p. 123531, Jun. 2010.
[16] A. Needleman, "An analysis of decohesion along an imperfect interface," *Int. J. Fracture*, vol. 42, no. 42, pp. 21–40, Jan. 1990.

Shutao Qiao received the bachelor's degree from Xi'an Jiaotong University, Xi'an, China, in 2012. He is currently pursuing the Ph.D. degree with the Prof. Nanshu Lu's Group, University of Texas at Austin, Austin, TX, USA, working on mechanics in the manufacture of flexible electronics.

Mr. Qiao received the Cockrell School of Engineering Eugene A. Ripperger Scholarship in 2013 and the UT Graduate School Bruton Fellowship in 2014.

Jean-Baptiste Gratadour received the M.S. degree in mechanical engineering from Arts et Métiers ParisTech, Paris, France, in 2014.

He has been with the University of Centrale Lille, Lille, France, since 2014. He has been a Visiting Student with the Prof. Nanshu Lu's Group, while he finished the project on modeling thin film conformability with corrugated substrate.

Liu Wang received the bachelor's degree from The University of Science and Technology of China, Hefei, China, in 2014. He is currently pursuing the Ph.D. degree with the Prof. Nanshu Lu's Group, University of Texas at Austin, working on the mechanics of bio-electronics interface.

Mr. Wang received the 2015-2016 Raynor L. Duncombe Endowed Fellowship in aerospace engineering

Nanshu Lu received the bachelor's degree from Tsinghua University, Beijing, China, in 2005, and the Ph.D. degree from Harvard University, Boston, MA, USA, in 2009.

She has been a Beckman Post-Doctoral Fellow with the University of Illinois. She joined the University of Texas at Austin, Austin, TX, USA, in 2011, as an Assistant Professor. She has over 40 journal publications with more than 2000 citations in the field of thin-film mechanics and flexible electronics.

Dr. Lu was named 35 innovators under 35 by MIT Technology Review, and received the NSF CAREER Award, the AFOSR Young Investigator Award, the ONR Young Investigator Award, and the 3M Non-Tenured Faculty Award.